CHAPTER 1

MIDDLE CEREBRAL ARTERY ANEURYSM COIL POROSITY ANALYSIS ON STENOSIS FORMATION USING CFD MECHANICS

Nadia Shaira Shafii[1,5], Takahisa Yamamoto[3], Ikram Sufian Bin Hamza[2], Kahar Osman[2,5] and Nofrizalidris Darlis[4]*

[1]Department of Biomedical Engineering and Health Sciences, Faculty of Electrical Engineering, Universiti Teknologi Malaysia, 81310 Johor, Malaysia

[2]Faculty of Mechanical Engineering, Universiti Teknologi Malaysia, 81310 Johor, Malaysia

[3]National Institute of Technology, Gifu College, Japan

[4] Centre of Automotive & Powertrain Technology, Faculty of Engineering Technology, University Tun Hussein Onn Malaysia, Edu Hub Pagoh, 84600, Muar, Johor, Malaysia

[5]IJN-UTM Cardiovascular Engineering Center, Institute of Human Centered Engineering, Universiti Teknologi Malaysia, 81300 Skudai Johor

1.1 INTRODUCTION

The anterior cerebral circulation includes the middle cerebral artery (MCA), which is a terminal branch of the internal carotid artery. Many deep brain structures, as well as the bulk of the lateral surface of the cerebral hemispheres and the temporal pole of the brain, are supplied by the middle cerebral artery. It flows from the base of the brain to the lateral sulcus (of Sylvius), where it terminates on the brain's lateral surface. The procedure separates the middle cerebral artery into four segments (M1-M4) that branch out into a total of branches. The internal carotid artery enters the interpeduncular fossa from the lateral angle of the circle of Willis and branches into the middle cerebral artery. It runs between the frontal and temporal lobes, passing through the Sylvian fissure. It next reaches the insula's posterosuperior surface, where it splits into superior and inferior trunks. The trunks pass through the Sylvian fissure together on their way to the lateral surface of the brain. The middle cerebral artery can be divided into four segments to assist identify its path. The M1 (sphenoidal/horizontal) segment runs virtually horizontally from the internal carotid artery to a point where the MCA bifurcates between the temporal and frontal lobes. It is found in the Sylvian fissure's sphenoidal segment, where it runs all the way to the Sylvian fissure's sphenoidal and operculoinsular segment's junction. The branches of the middle cerebral artery make a 90° turn in the poster superior direction at the point of M1 segment termination, which is known as the genu (lat. "knee") of the middle cerebral artery. The superior and inferior trunks of the main cerebral artery split here.

The superior and inferior trunks of the M2(insular) segment begin at the bifurcation of the middle cerebral artery. This stretch begins at the genu of MCA at the level of the limen insulae and continues along the insula's surface. It ends at the level of the insula's circular sulcus. M3(opercula) segments begin at the point where they ascend from the insula's circular sulcus to the brain's surface. This segment runs along the inner surfaces of the insular operculum's parietal and temporal portions. Once it emerges through the lateral fissure to reach the surface of the brain and travels along the surface of the cerebral hemisphere, M4 (terminal, cortical) segments continue onto the M3 segment. The most common site of atherosclerotic intracranial arterial stenosis is in the middle cerebral artery. MCA stenosis results in brain infraction and is linked to recurrent stroke. Atherosclerosis is a vascular disease that causes plaque deposition and arterial wall thickening, reducing the size of the artery lumen. Heart disease and stroke, which are pathological consequences of atherosclerosis, are still the world's leading causes of death. The most common cause of stroke is stenosis in the coronary artery, which prevents oxygen from reaching the organs and causes paralysis. All large and medium arteries can be affected by atherosclerosis. The cardiovascular system's branches and bends have a higher possibility of producing blood clots. Lipid, inflammatory cells, smooth muscle cells, and connective tissue make up atherosclerotic plaques. Diabetes, cigarette smoking, family history, sedentary lifestyle, obesity, and hypertension are all risk factors for this condition. Aside from variables, local hemodynamic factors including wall shear stress play an important role in the formation of atherosclerotic plaques. According to statistics, coronary and cerebral atherosclerosis caused more than 650,000 deaths in the United States in 2001. This figure is nearly six times that of cancer and nearly six times that of accidents. The unpredictability of blood flow is well established. The cyclic structure of the MCA causes the temporary phenomena of blood flow. That is, the velocity and pressure conditions fluctuate with time at a particular place. Blood velocity in the circulatory system is pulsing, varying between zero during diastole and high speeds during systole. Blood flow is laminar, but when the artery diameter and velocities are great for arteries like the aorta, it becomes turbulent due to the pulsing nature of the flow. These complex hemodynamic characteristics of blood flow play an important role in forming the atherosclerotic plaques. The computational fluid dynamic (CFD) method is extensively utilised for flow analysis via stented arteries because it is an effective tool for analysing the micro characteristics involved in the flow. Computational fluid dynamics (CFD) software tool analyses fluid flow using a mathematical model of the physical situation and numerical methods. A mathematical model varies in accordance with the content of the problem such as heat transfer, mass transfer, phase change and etc.

1.2 METHODOLOGY

1.2.1 Geometry

From Figure. 1.1 and Figure. 1.2, the flow project procedure will start with background study and literature review on the flow analysis in middle cerebral artery with stenosis. Based on the review, the fractional pressure ratio is introduced to assess the hemodynamic significance of severe middle cerebral artery stenosis. In this study, Takao et al. [31] the methods used were clinical cases and computational fluid dynamic modelling.

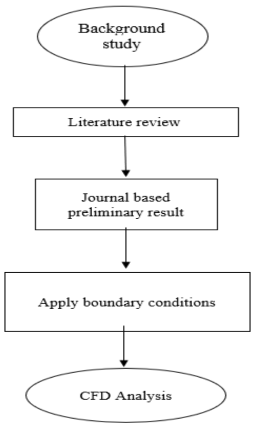

Figure 1.1: Flowchart for general research methodology

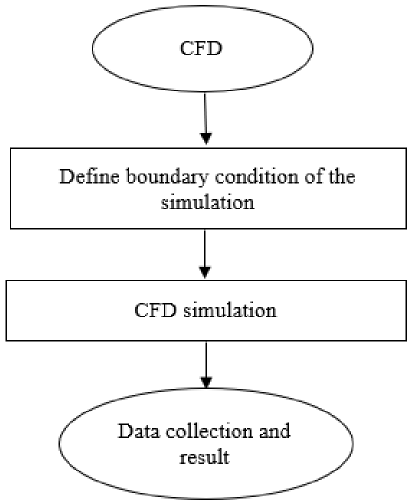

Figure 1.2: Flowchart for CFD of the research methodolog

1.2.2 Clinical Cases

Takao et al. [31] review about patients with unruptured arteries (UAs) who were waiting for surgery or who declined surgery had their arteries ruptured in 13 cases (internal carotid artery 7, middle cerebral artery 6). In this study, they called the aneurysms "ruptured aneurysms (RAs)." The diameters of all burst aneurysms ranged from 5 to 10 mm, with an average of 6.21 mm for RA in the middle cerebral artery.

1.2.3 Computational Fluid Dynamic Modelling

The application of computational techniques in the investigation of the blood flow in arteries has become an important tool due to its ability to stimulate velocity and pressure fields in virtual models of the middle cerebral artery functionality. CFD studies can go further by visualizing the flow, wall shear stress (WSS) mass transport, and stagnation regions which is difficult to show or describe by using experimental techniques. The simulation of CFD will focused on blood flow of unruptured (healthy) and ruptured (atherosclerotic) arteries. Takao et al. [31] stated that the geometry of blood arteries was recovered from head CT angiography pictures using manual cropping, image thresholding, and conversion to a triangulated surface using "Real Intage." A triangulated surface was used to create an unstructured mesh. The mesh was mostly made up of tetrahedrons, with multiple layers of prism elements employed along the wall surface to improve the boundary layer's analytic precision. The Navier-Strokes equations were used to stimulate blood flow on the computational mesh under the assumptions of pulsatile laminar flow, zero pressure at the blood vessel outlet, Newtonian fluid, and solid blood vessel walls with nonslip condition. For mesh generation and fluid simulation, commercial software (ANSYS ICEM CFD 12.1) was used.

For RA, the latest CT angiography image available before rupture was used. For UA, the latest CT angiography image acquired during follow-up was used. Wall shear stress (WSS) and oscillatory shear index (OSI) and 2 additional hemodynamic parameters, energy loss (EL) and pressure loss coefficient (PLc), which are associated with the expenditure flow energy in the aneurysm region.

Table 1.1: Table of CFD modelling parameter

CFD Modeling Parameter		Unit
Density, p	1060	Kg/m3
Viscosity, µ	0.00345	Pa.s
Mesh element Number	600271	Elements

Energy loss is EL per unit volume, and it comprehensively represents energy expenditure due to viscous frictions and whirlpool formation.

$$\boldsymbol{EL} = \frac{\boldsymbol{v_{in}A}.((\frac{1}{2}\boldsymbol{pv^2}_{in}+\boldsymbol{P}_{in})-(\frac{1}{2}\boldsymbol{pv^2}_{out}+\boldsymbol{P}_{out})}{\boldsymbol{v_m}} \quad (1)$$

P is the fluid density, $\boldsymbol{v_{in}}$ represents the volume of the measurement section and Ain is the area of the test plane at the inlet of the measurement region. V_{in} and P_{in} represent mean flow velocity and statistic pressure of the test plane at the inlet side respectively for v_{out} and $\boldsymbol{P_{out}}$ for at outlet side. Pressure loss coefficient is a dimensionless quantity representing pressure loss,

$$\boldsymbol{PLc} = \frac{\Delta \boldsymbol{P}}{\frac{1}{2}\boldsymbol{pv^2}_{in}} \quad (2)$$

$\frac{1}{2}\boldsymbol{pv^2}_{in}$ is the dynamic pressure and $\Delta \boldsymbol{P}$ is the pressure loss which is

$$\Delta \boldsymbol{P} = \left(\frac{1}{2}\boldsymbol{pv^2}_{in} + \boldsymbol{P}_{in}\right) - (\frac{1}{2}\boldsymbol{pv^2}_{out} + \boldsymbol{P}_{out}) \quad (3)$$

Pressure loss due to viscous friction and whirlpool formation in the measurement region and therefore, related to energy expenditure.

1.2.4 Modelling

There are 4 models of the middle cerebral artery (MCA) were developed using computer-aided design (CAD) in SolidWorks software, as illustrated in Figure 1.3. These models include a healthy MCA, an MCA with an aneurysm, and two coiled MCA aneurysm models with different coil porosities, namely 50% and 70%. The variations in geometry and coil density were constructed to analyze the hemodynamic and structural effects of aneurysm formation and endovascular coiling treatment on the MCA.

1.2.5 Meshing

A three-dimensional tetrahedral mesh consisting of approximately 600,271 nodes was generated to discretize the model geometry for finite element analysis. The tetrahedral elements were selected due to their ability to accurately capture complex and irregular geometries, ensuring adequate representation of curved surfaces and localized stress regions as in Figure 1.3.

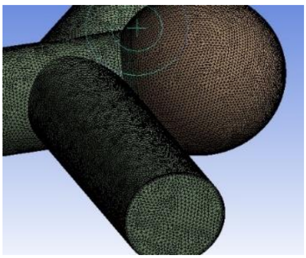

Figure 1.3: Meshing of MCA with aneurysm

1.2.6 Boundary Condition

The MCA's outer wall is believed to be rigid and without a slip condition. The velocity table created from the physically realistic waveform generates the inlet boundary condition as in Table 1.2. The obtained systolic peak velocity and diastolic velocities are listed in Figure 1.4. Zero pressure is given as the output boundary condition.

Table 1.2 Boundary Conditions

Inlet Pressure, Pa	**Velocity profile, transient mode**
Outlet Pressure, Pa	0
Blood density, p	1060
Blood viscosity, µ	
Normal condition used (Azhim et al (2013).	

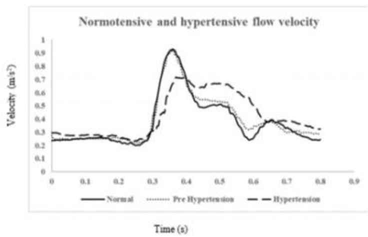

Figure 1.4: Normotensive and Hypertensive flow velocity

1.2.7 Boundary Condition

Several parameters were analyzed in this study, including velocity contour, vortex distribution, wall shear stress, and pressure drop. These parameters are essential for evaluating the influence of coil porosity on blood flow characteristics within the middle cerebral artery (MCA) aneurysm models. By examining these factors, the study aims to better understand the hemodynamic behavior and treatment effectiveness associated with different coil porosities, ultimately contributing to the achievement of the research objectives.

1.3 RESULTS AND DISCUSSION

The output of the Ansys simulation was compared to selected experimental data at this stage of the project. Within the middle cerebral artery aneurysm coil porosity, the simulation was used to determine the velocity contour, vortex dispersion, wall shear stress, and pressure drop.

1.3.1 Velocity Distribution

Over time, a stenosis-affected arterial zone may emerge around the branch's entrance. Healthy MCA, MCA with aneurysm, and a region with 50% and 70% porosity limitation in the flow region was used to characterize the flow in a stenosis affected region. For velocity contour, a method of determining stream discharge in which point velocity measurements are contoured to yield average cross-sectional flow velocities, which are then multiplied by the areas of the cross sections to yield the discharge. The flow disturbances induced by the stenosis impacted artery's CFD simulation results highlight the flow disturbances caused by the flow limitation. Figure 1.5 illustrates the flow distribution of the aneurysm in MCA at peak 0.325 sec.

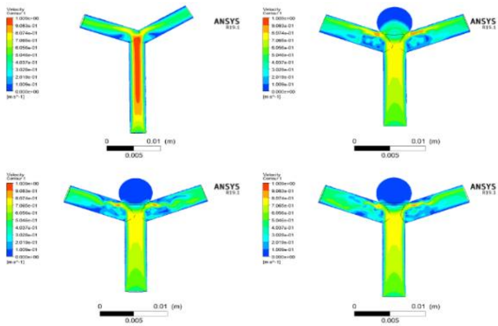

Figure 1.5 Velocity distribution at 0sec, 0.125sec, 0.325 sec and 0.375 sec

The flow disruptions generated by the artery limitation can be seen in 0.325sec. We can see from the flow patterns that there is more recirculation zones produced at the branch's entrance than in a healthy artery. It can be established that the flow patterns along the middle cerebral artery are highly variable. The presence of flow separation can be seen in the flow at the branch's entrance. We may deduce from these flow patterns that while it may take a long time to initiate plaque formation, it takes less time to raise the proportion of restriction as well as growth in the leading and trailing ends once the restriction has been formed.

1.3.2 Vortex Distribution

Vortex distribution is a region in a fluid where the flow spins around an axis line, which can be straight or curved, in fluid dynamics. Turbulent flow is characterized by vortices. Vortices are defined by their velocity distribution, vorticity (the curl of the flow velocity), and the idea of circulation. The fluid flow velocity in most vortices is greatest near the axis and decreases in inverse proportion to distance from the axis. Figure 1.7 illustrates the vortex distribution of the aneurysm in MCA at peak.

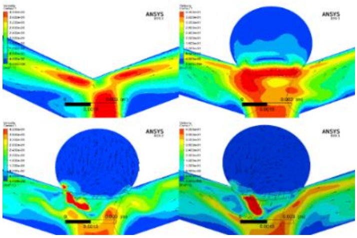

Figure 1.6: Vortex distribution at 0sec, 0.125sec, 0.325 sec and 0.375 sec

1.3.3 Pressure Difference

The difference in total pressure between two sites in a fluid-carrying network is known as pressure drop. Pressure drop, or pressure loss, occurs when a liquid material enters one end of artery system and exits the other. The maximum pressure (P_{max}) at the coil plane, average pressure (P_{ave}) at the inlet plane, average velocity (V_{in}) is 0.495023 at the inlet plane, and pressure difference (PD) were measured. P_{max}, P_{ave}, and V_{in} are components of PD. P_{max} was calculated as the highest value of pressure in the virtual and real coil planes. Pave was calculated as the mean value of the pressure at the inlet plane. Vin was calculated as the average flow velocity at the inlet plane in meters per second. These values were analysed at the peak systole. It can be concluding that the pressure difference was not the same as the values get from the calculation were different. As the maximum pressure for coiled MCA aneurysm with 50% porosity are higher compared to the other three models of MCA. The pressure difference is much greater. Results show as in Table 1.3.

Table 1.3 Calculated values of pressure drop in 4 models of MCA

Model	P_{ave}	P_{max}	$(V_{in})2$	***Pressure difference (PD)***
No aneurysm	208.578	0	0.245048	0
With aneurysm	338.031	487.954	0.245048	1.173
Coiled MCA aneurysm (50%)	363.62	6095.22	0.245048	45.1
Coiled MCA aneurysm (70%)	367.158	1331.42	0.245048	7.59

1.3.4 Wall shear stress

Wall shear stress, fluid does not move at the same velocity at every location in a straight vessel in nonpulsatile flow. Fluid flow, on the other hand, is fastest in the centre and slowest along the wall. The fluid velocities take on a "laminar flow" profile, which is a parabolic profile. The fluid viscosity is connected to this flow pattern, which is caused by friction within the fluid and between the fluid and the vessel wall. The "wall shear stress" is a tangential force exerted by the moving fluid as a result of this friction. The magnitude of wall shear stress is determined by the rate at which fluid velocity increases as it moves from the vessel wall to the centre. The WSS acting on the MCA walls is plotted against the time. Shear stress plots at each time steps selected are shown in the Figure 1.8. There was no statistically significant difference between healthy MCA and MCA with aneurysm cases. Based on Table 1.4 at 0.325 sec, at coiled MCA aneurysm 50% porosity the maximum wall shear stress (WSS) is 5809.75 Pa which is the highest compared to other 3 MCA models In the tiny aneurysm area of all ruptured cases, high and low WSS were intermingled. In ruptured cases, blood from the parent artery flowed more directly into the aneurysm, resulting in high WSSs at the aneurysm's body or neck. In ruptured cases, this resulted in a higher averaged WSS of the aneurysm region. As the maximum wall shear stress are different in each types of MCA due to the present of aneurysm. When the spatially averaged WSS of the aneurysm region at peak systole was examined between ruptured and unruptured cases, it was discovered that the ruptured cases had a considerably greater WSS. So, the increase in the porosity will increase the wall shear stress in ruptured cases.

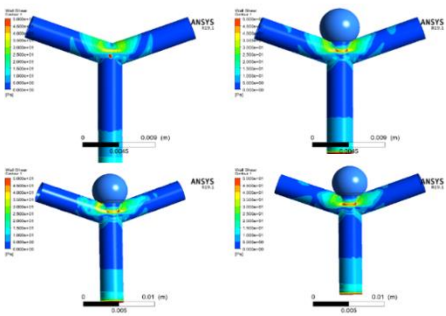

Figure 1.8: Wall Shear Stress (WSS) MCA Aneurysm at 0.325se

Table 1.4: Maximum Wall Shear Stress (WSS) on the MCA

Time (s)	0.1s	0.25s	0.325s	0.375s
No aneurysm	2081.29 Pa	1566.67 Pa	1944.58 Pa	1973.22 Pa
With aneurysm	57.411 Pa	206.045 Pa	135.447 Pa	67.87 Pa
Coiled MCA aneurysm (50%)	5065.17 Pa	5809.75 Pa	2825.38 Pa	2894.03 Pa
Coiled MCA aneurysm (70%)	5563.13 Pa	7850.26 Pa	7454.9 Pa	7956.1 Pa

1.4 CONCLUSION

Using commercial software, a computational fluid dynamic (CFD) analysis of the middle cerebral artery is performed by assuming blood flow as a pulsing, incompressible, and Newtonian flow over a realistic velocity waveform of the middle cerebral artery. Ansys 19.0 is a computer simulation software. Healthy middle cerebral artery, middle cerebral artery with aneurysm, coiled middle cerebral artery aneurysm with 50%and 70% porosity were all used in simulations. For these structures, the velocity contour, vortex distribution, wall shear stress and pressure drop across the MCA cycle are analysed.

The complex blood flow pattern with slow moving regions, as well as the flow patterns in the arteries, are highly modifying along the MCA cycle. During the MCA cycle, flow separation and circulatory regions form near the wall, which is a primary contributor to the formation of atherosclerotic plaque at that location. It may take a long time for plaque to form, but once it does, the plaque can quickly grow in size and block the artery. The pressure in the middle cerebral artery due to the aneurysm will affect the velocity distribution as the flow pattern for each model are different. It can be concluded that the presence of aneurysm affects the blood flow which increasing the pressure in middle cerebral artery. As the maximum wall shear stress are different in each types of MCA due to the present of aneurysm. When the spatially averaged WSS of the aneurysm region at peak systole was examined between ruptured and unruptured cases, it was discovered that the ruptured cases had a considerably greater WSS. So, the increase in the porosity will increase the wall shear stress in ruptured cases.

BIBLIOGRAPHY

[1] K. D. Ku, “Blood flow in arteries,” Annu. Rev. Fluid Mech., vol. 29, pp. 399–434, 1997.

[2] L. Zarrinkoob, K. Ambarki, A. Wåhlin, A. Birgander, R. Eklund, and A. Malm, “Blood flow distribution in cerebral arteries,” J. Cereb. Blood Flow Metab., vol. 35, no. 11, pp. 648–654, 2015.

[3] N. A. Lassen, “Blood flow and oxygen,” Physiol. Rev., vol. 39, no. 2, pp. 183–238, 1959.

[4] K. Hachinski et al., “Cerebral blood flow in dementia,” Arch. Neurol., vol. 32, no. 9, pp. 632–637, 1975.

[5] M. A. Heymann, D. B. Payne, J. E. Rudolph, and A. M. Rudolph, “Blood flow measurements with radionuclide-labeled particles,” Prog. Cardiovasc. Dis., vol. 20, no. 1, pp. 55–79, 1977.

[6] M. Reichle, J. E. Pourser, J. B. Plum, and F. Plum, “Cerebral blood flow during coma,” Arch. Neurol., vol. 23, no. 5, pp. 394–403, 1970.

[7] D. Attwell, A. M. Buchan, R. Charpak, S. Lauritzen, M. Macvicar, and E. A. Newman, “Glial and neuronal control of brain blood flow,” Nature, vol. 468, no. 7321, pp. 232–243, 2010.

[8] E. C. Peterson, Z. Wang, and Z. Britz, “Regulation of cerebral blood flow,” Int. J. Vasc. Med., vol. 2011, Art. no. 823525, 2011.

[9] S. On, “Studies on the velocity of blood flow: I. The method utilized,” Am. Heart J., vol. 2, no. 5, pp. 583–590, 1927.

[10] J. Liu et al., “Functional assessment of cerebral artery stenosis: A pilot study based on computational fluid dynamics,” J. Cereb. Blood Flow Metab., vol. 37, no. 7, pp. 2567–2576, 2017.

[11] J. Liu et al., “Functional assessment of the stenotic carotid artery by CFD-based pressure gradient evaluation,” Am. J. Physiol. Heart Circ. Physiol., vol. 311, no. 3, pp. H645–H653, 2016.

[12] A. Polanczyk, M. Podgorski, T. Wozniak, T. Stefanczyk, L. Strzelecki, and K. Strzelecki, “Computational fluid dynamics as an engineering tool for the reconstruction of hemodynamics after carotid artery stenosis operation: A case study,” Medicina, vol. 54, no. 3, Art. no. 42, 2018.

[13] C. Derdyn, C. P. Powers, W. J. Grubb, and R. L. Grubb, “Hemodynamic effects of middle cerebral artery stenosis and occlusion,” Rivista di Neuroradiologia, vol. 11, Suppl. 2, pp. 211–215, 1998.

[14] H. Rajabzadeh-Oghaz, H. van Ooij, S. P. Veeturi, V. M. Zuinno, J. J. M. Zwannenburg, and H. Meng, "Inter-patient variations in flow boundary conditions at the middle cerebral artery from 7T PC-MRI and influence on computational fluid dynamics of intracranial aneurysms," Comput. Biol. Med., vol. 120, Art. no. 103759, 2020.

[15] M. Holmgren, K. M. Støvrud, L. Zarrinkoob, A. Wåhlin, A. Malm, and J. Eklund, "Middle cerebral artery pressure laterality in patients with symptomatic ICA stenosis," PLoS One, vol. 16, no. 1, Art. no. e0245337, 2021.

[16] S. Razavi, E. Farhangmehr, V. Zendeli, and N. Zendeli, "Numerical investigation of the blood flow through the middle cerebral artery," BioImpacts, vol. 8, no. 3, pp. 195–200, 2018.[17] S. Sia, Z. F. Zhang, Y. Qian, Y. Kadir, K. A. A. Nor, H. M. Rahman, and M. K. Morgan, "Hemodynamic effects resulting from a common carotid to middle cerebral bypass with varying degrees of proximal internal carotid stenosis," Neurology Asia, vol. 19, no. 3, pp. 241–247, 2014.

[18] K. Fukazawa et al., "Using computational fluid dynamics analysis to characterize local hemodynamic features of middle cerebral artery aneurysm rupture points," World Neurosurg., vol. 83, no. 1, pp. 80–86, 2015.

[19] N. Olewnja, S. Lee, C. J. Ishihara, S. Y. Yamane, F. Zhang, Y. Qian, and Y. Qian, "Analysis of restenosis after carotid artery stenting: Preliminary results using computational fluid dynamics based on three-dimensional angiography," J. Clin. Neurosci., vol. 20, no. 11, pp. 1582–1587, 2013.